Fundamental accuracy of time domain finite element method for sound-field analysis of rooms

Okuzono, Takeshi

Otsuru, Toru

Tomiku, Reiji

Okamoto, Noriko

(Citation)
Applied Acoustics,71(10):940-946

(Issue Date)
2010-10

(Resource Type)
journal article

(Version)
Accepted Manuscript

(URL)
https://hdl.handle.net/20.500.14094/90005723

Fundamental accuracy of time domain finite element method for sound field analysis of rooms

Takeshi Okuzono[a,1] Toru Otsuru[b], Reiji Tomiku[b], Noriko Okamoto[c]

[a] *Graduate School of Engineering, Oita University, 700 Dannoharu, Oita 870-1192, Japan*

[b] *Department of Architecture and Mechatronics, Architecture Course, Faculty of Engineering, Oita University, 700 Dannoharu, Oita 870-1192, Japan*

[c] *Venture Business Laboratory, Oita University, 700 Dannoharu, Oita 870-1192, Japan*

Abstract

This paper presents an assessment of the accuracy and applicability of a time domain finite element method (TDFEM) for sound-field analysis in architectural space. This TDFEM incorporates several techniques: (1) a hexahedral 27-node isoparametric acoustic element using a spline function; (2) a lumped acoustic dissipation matrix; and (3) Newmark time integration method with an absolute diagonal scaled COCG iterative solver. Sound fields in an irregularly shaped reverberation room of 166 m^3 are computed using TDFEM. The computed values and measured values for 125–500 Hz are compared, revealing that the fine structure of the computed band-limited impulse responses agree with measured ones up to 0.1 s, with a cross correlation coefficient greater than 0.93. The cross correlation coefficient decreases gradually over time, and more rapidly for higher frequencies. Moreover, the computed decay curves, and the reverberation times, agree well with the respective measured ones, and with a better fit the higher the frequency (up to 500 Hz).

Key words: Room acoustics, Sound field analysis, Time domain finite element method, Accuracy

[1] Corresponding author. Tel./fax: +81 97 554 6406/7918.
E-mail address: okuzono@cc.oita-u.ac.jp (T. Okuzono).

1. Introduction

Numerical analysis methods based on wave acoustics (Wave-based methods) such as finite element method (FEM) and boundary element method are powerful numerical methods used to predict sound fields in architectural space accurately with complicated boundary conditions. Generally, a wave-based method entails large computational cost for analyzing sound fields in architectural space with practical dimensions as well as practical frequency ranges. However, recently, the application of wave-based methods is increasing gradually along with the rapid progress of computer technology.

Although both time and frequency domain analyses using wave-based methods are conducted for predicting sound fields in architectural spaces, time domain analysis is straightforward in calculating the impulse response of the space in a time domain without the use of inverse Fourier transform. Various acoustical parameters used for acoustical quality evaluation are calculable from the impulse response.

The finite-difference time-domain (FDTD) method is a widely used method of computing the impulse response in a space[1, 2, 3]. The explicit formulation makes the computation efficient, and the computational effort increases linearly in direct relation to the number of discretization cells. However, the architectural space boundary shape is approximated by a staircase approximation in many cases, which is a disadvantage of the FDTD method because a room's shape is an important factor to determine acoustic properties in an architectural space.

Because it enables modeling of complicated boundary shape, FEM is an attractive method. Various methods incorporating FEM are used for computing the impulse response in a space: indirect method with inverse Fourier transform of frequency domain response computed using frequency domain FEM (FDFEM)[4], a method using FEM with a modal analysis approach[5, 6], and a direct method using time domain FEM (TDFEM) with direct time integration method[7, 8].

Among them, TDFEM can treat time variation of the boundary condition and medium. Although this method typically requires a solution technique of a linear system of equations at each time step, the matrices arising from the finite element formulation are generally sparse. Therefore, using a Krylov subspace iterative solver such as the Conjugate Gradient (CG) method, the memory and operations required for TDFEM can be reduced approximately to the order of degrees of freedom (DOFs) of the finite element model, if

a fast convergence of the iterative solver can be expected. In addition, using the unconditionally stable direct time integration method, TDFEM has unconditional stability. Therefore, if TDFEM provides a similarly accurate result as the FDTD method using fewer elements per wavelength and a much larger time interval, which engenders a decrease of DOFs and total number of time steps compared to those required for the FDTD method, then the computational costs for the TDFEM would be favourable compare to those required for the FDTD method. Moreover, TDFEM is well suited to vector and/or parallel computation, which is also the case for the FDTD method. Nevertheless, few studies have examined application of TDFEM for sound field analyses in architectural spaces.

To reduce the computational cost of the TDFEM and to use a method for practical situations such as the design process of a room and acoustic improvement of an existing room, the authors developed TDFEM, including the following techniques[9]: (1) hexahedral 27-node isoparametric acoustic element using spline function[10, 11], (2) lumped acoustic dissipation matrix, and (3) Newmark time integration method with absolute diagonal scaled COCG Krylov subspace iterative solver. Moreover, the authors have already shown that the linear system of equations can be solved efficiently using the iterative solver[9, 12].

However, accuracy and applicability of the TDFEM to sound field analyses in architectural space remain unclear. Consequently, this study was undertaken to assess the basic accuracy and applicability of the TDFEM for sound field analysis in architectural space through comparison with measured values.

This paper is organized as follows. Section 2 presents outlines of both mathematical and physical bases of the presented TDFEM. In Sec. 3, we present a comparison of computed and measured results of a sound field in an irregularly shaped reverberation room with volume of 166 m^3. Finally, in Sec. 4, we present concluding remarks.

2. Sound field analyses using time domain finite element method: TDFEM

Following a standard finite element procedure based on the principle of minimum total potential energy applied to a three-dimensional sound field,

the following discretized matrix equation in the frequency domain is obtained.

$$[K]\{p\} + \mathrm{i}\omega[C]\{p\} - \omega^2[M]\{p\} = \mathrm{i}\omega\rho v_0\{W\} \tag{1}$$

Therein, $[M]$, $[C]$, and $[K]$ respectively denote acoustic mass, dissipation, and stiffness matrices. Furthermore, i, $\{p\}$, ρ, ω, v_0, and $\{W\}$ respectively signify an imaginary unit (i^2 = -1), sound pressure vector, the air density, angular frequency, the particle velocity and distribution vector. Assuming that $\cdot$ and $\cdot\cdot$ respectively signify first-order and second-order derivatives with respect to time, the semi-discrete equation in the time domain can be expressed as presented below.

$$[M]\{\ddot{p}\} + [C]\{\dot{p}\} + [K]\{p\} = \rho\dot{v_0}\{W\} \tag{2}$$

Using an interpolation function $N(x, y, z)$, the sound pressure $p(x, y, z)$ on an arbitrary point at (x, y, z) is assumed to be

$$p(x, y, z) = \{N(x, y, z)\}^T\{p\}_e. \tag{3}$$

The analysis described in this paper uses a hexahedral 27-node isoparametric acoustic element with the spline polynomial function for $N(x, y, z)$[10, 11]. Acoustic element matrices used to construct global matrices in Eq. (1) are given as expressed below.

$$[K]_e = \int_e \left(\{\frac{\partial N}{\partial x}\}\{\frac{\partial N}{\partial x}\}^T + \{\frac{\partial N}{\partial y}\}\{\frac{\partial N}{\partial y}\}^T + \{\frac{\partial N}{\partial z}\}\{\frac{\partial N}{\partial z}\}^T \right) dV, \tag{4}$$

$$[M]_e = \frac{1}{c^2}\int_e \{N\}\{N\}^T dV, \tag{5}$$

$$[C]_e = \frac{1}{c}\int_{e'} \frac{1}{z_n}\{N\}\{N\}^T dS \tag{6}$$

Herein, c and z_n respectively represent the speed of sound and normal surface impedance; e' denotes the surface area to be integrated. As described in this paper, a locally reactive model is assumed for dissipation; then, $[C]_e$ can be reassembled into a diagonal matrix as the lumped acoustic dissipation matrix.

In the time domain, Newmark β method[13] is used to solve Eq. (2) step by step. If $\{p\}_t$, $\{\dot{p}\}_t$ and $\{\ddot{p}\}_t$ at time t are known, then $\{p\}_{t+\Delta t}$ and $\{\dot{p}\}_{t+\Delta t}$ can be given as

$$\{p\}_{t+\Delta t} = \{p\}_t + \Delta t\{\dot{p}\}_t + (\Delta t)^2(\frac{1}{2} - \beta)\{\ddot{p}\}_t + (\Delta t)^2\beta\{\ddot{p}\}_{t+\Delta t}, \quad (7)$$

$$\{\dot{p}\}_{t+\Delta t} = \{\dot{p}\}_t + \Delta t(1-\gamma)\{\ddot{p}\}_t + \Delta t\gamma\{\ddot{p}\}_{t+\Delta t}. \quad (8)$$

In those equations, Δt is the time interval between t and $t+\Delta t$, and γ, β are parameters related to the accuracy and stability of the method. For this study, γ is set to $1/2$ to maintain the second-order accuracy. Then, with the Eqs. (7) and (8), it is possible to transform Eq. (2) into

$$\Big[[M] + \frac{\Delta t}{2}[C] + \beta(\Delta t)^2[K]\Big]\{\ddot{p}\}_{t+\Delta t} = \{f\}_{t+\Delta t} - [C]\{P\} - [K]\{Q\}, \quad (9)$$

where

$$\{P\} = \{\dot{p}\}_t + \frac{\Delta t}{2}\{\ddot{p}\}_t, \{Q\} = \{p\}_t + \Delta t\{\dot{p}\}_t + (\frac{1}{2} - \beta)(\Delta t)^2\{\ddot{p}\}_t. \quad (10)$$

Consequently, $\{\ddot{p}\}_{t+\Delta t}$ is calculable by solving Eq. (9). Finally, the sound pressure $\{p\}_{t+\Delta t}$ and first derivative of the sound pressure $\{\dot{p}\}_{t+\Delta t}$ are calculable respectively by substituting $\{\ddot{p}\}_{t+\Delta t}$ into Eq. (7) and Eq. (8).

Several Newmark methods exist with different values of parameter β[14]. The following three special cases of the Newmark methods are well known: constant average acceleration method with β=1/4, linear acceleration method with β=1/6, and Fox–Goodwin method with β=1/12. Here, if $\beta \geq 1/4$, then the Newmark method is unconditionally stable.

Moreover, the Newmark method usually requires solution of the linear system of equations with Eq. (9) at each time step. As a shorter expression, Eq. (9) can be rewritten as

$$[A]\{\ddot{p}\}_{t+\Delta t} = \{b\}_{t+\Delta t}. \quad (11)$$

Therein, $[A]$ and $\{b\}_{t+\Delta t}$ respectively denote the coefficient matrix and the right-hand side vector in Eq. (9). When z_n is given as a complex number, $[A]$ becomes a complex sparse symmetric matrix—a non-Hermitian—because $[K]$ and $[M]$ are real sparse symmetric matrices; $[C]$ is a complex diagonal matrix. As a special case, when z_n is given as a real number for simplification, $[A]$ becomes a real symmetric matrix. Then, to solve eq. (11), we adopt

Conjugate Orthogonal Conjugate Gradient (COCG) method[15], which is the efficient iterative solver for the FEM formulation in [9], and which is also used here. This method is equivalent to CG method when $[A]$ becomes a real symmetric matrix. As a preconditioning technique, the absolute diagonal scaling[16], not increasing the number of complex component in the $[A]$, is used. Using preconditioning, the scaled matrix $[A]$ is written as

$$a'_{ij} = \frac{a_{ij}}{\sqrt{|a_{ii}|}\sqrt{|a_{jj}|}}, \tag{12}$$

where a_{ij} and a'_{ij} are components of $[A]$ before and after preconditioning. This preconditioned COCG method is well suited to parallelization. Using the relative residual 2-norm δ, the stopping criterion for stopping the succession of iterations of the COCG method is used as

$$\delta = \frac{||[A]\{\ddot{p}_n\}_{t+\Delta t} - \{b\}_{t+\Delta t}||_2}{||\{b\}_{t+\Delta t}||_2} \leq 10^{-6}, \tag{13}$$

where $||\cdot||_2$ and $\{\ddot{p}_n\}_{t+\Delta t}$ are the 2-norm and solution vectors on n-th iteration.

3. Comparisons of band-limited impulse response and related acoustical quantities obtained by TDFEM and by measurement.

Sound fields in an irregularly shaped reverberation room with a lightly damped wall were computed to show the basic accuracy and the applicability of the TDFEM. The results were compared with measured ones.

The reverberation room to be computed and measured here is depicted in Fig. 1. The volume and the surface area of the room are, respectively, 166 m^3 and 179 m^2. Inner walls of the room are made of concrete.

We measured impulse responses at 60 receiving points, as shown in Fig. 1 using time stretched pulse (TSP) method[17]. The sampling frequency was 44.1 kHz. Synchronous averaging was performed three times. Synchronous averaging was used since the temperature fluctuation effect can be considered to be small for frequencies below 1 kHz[18]. An omnidirectional dodecahedral loudspeaker of 39 cm diameter (Type 4292; Brüel & Kjær) was placed at a height of 1.5 m, as depicted in Fig. 1. In addition, a 1/2-inch microphone

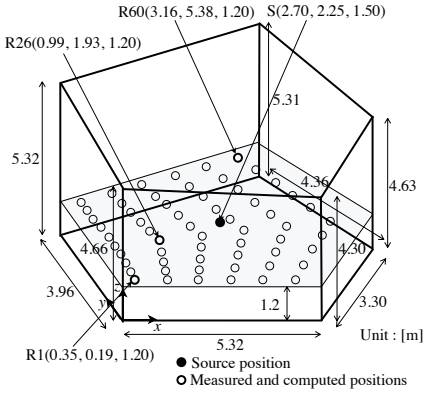

Figure 1: Schematic drawing of an irregularly shaped reverberation room with measured and computed points.

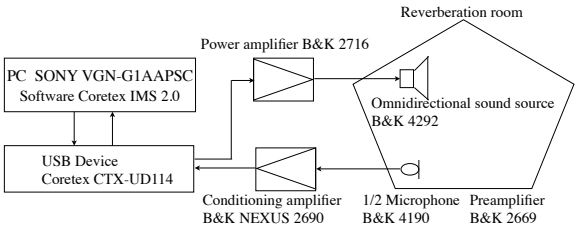

Figure 2: Impulse response measurement setup in the reverberation room.

(Type 4190; Brüel & Kjær) is placed 1.2 m above the floor, as depicted in Fig. 1. Figure 2 portrays a block diagram of the measurement.

Table 1 lists the measured reverberation times, their standard deviations and average absorption coefficients, $\overline{\alpha}$s, of the room surfaces with the frequency range of 125–500 Hz. The reverberation time is a spatial average value of 60 receiving points calculated using the integrated impulse response method. The evaluation range is 5–35 dB with the exception of 125 Hz. For 125 Hz, the range is 5–25 dB because a noise floor is observed. The values of $\overline{\alpha}$s were calculated by substituting measured reverberation times into the Sabine equation on the assumption that the sound field in the room is sufficiently diffuse. However, the Schroeder frequency of the reverberation room is approximately 505 Hz. This indicates that the sound field in the reverberation room is insufficiently diffuse below 500 Hz.

Table 1: Measured reverberation times, their standard deviations and average absorption coefficients of room surfaces calculated by substituting measured reverberation times into the Sabine equation.

	Frequency [Hz]		
	125	250	500
RT [s]	14.52	14.25	12.77
SD [s]	0.58	0.23	0.12
$\overline{\alpha}$	1.03×10^{-2}	1.05×10^{-2}	1.17×10^{-2}

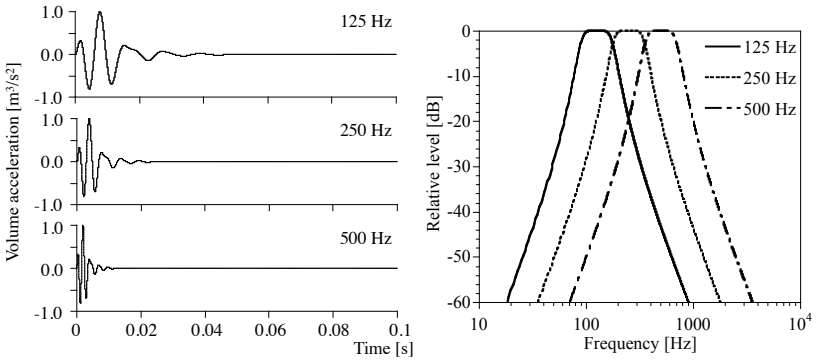

(a) Waveform (b) Frequency characteristic

Figure 3: Waveforms of sound sources and frequency characteristics for the FE analysis.

3.1. Setup of FE analysis

We computed band-limited impulse responses with octave bandwidths of center frequencies 125 Hz, 250 Hz, and 500 Hz at the 60 receiving points.

As a point source, the sound source is placed at 1.5 m height, as depicted in Fig. 1. The sound source signal used here is an impulse response of the IIR filter (Butterworth type band pass filter with third order). The source waveform and its frequency characteristics are depicted in Fig. 3.

Considering the incident condition of acoustic wave to the boundary surface, the normalized acoustic impedance ratios of wall surfaces were calculated by substituting $\overline{\alpha}$s of the walls into the following Eq. 14[19] of the random incidence absorption coefficient with the assumption that the normalized acoustic impedance ratio is independent of the incidence angle.

$$\overline{\alpha} = \frac{8}{z_e^2}[1 + z_e - \frac{1}{1 + z_e} - 2\ln(1 + z_e)]. \tag{14}$$

Table 2: Settings of FE analysis

Octave band center frequency [Hz]	DOF	Δt [ms]	T [s]	N_{step}
125	18,819	0.023	18.0	793,800
250	63,017	0.023	16.0	705,600
500	467,775	0.023	15.0	661,500

Therein, z_e denotes the normalized acoustic impedance ratio, but its imaginary part is set to zero, considering the nearly rigid concrete walls. Although another random incidence absorption coefficient using reverberant statistics and equivalent impedance of different types is presented in [19], we confirmed through preliminary investigation that the use of Eq. 14 performed better than absorption coefficients of another type. Therefore, we calculated z_e using Eq. 14 as a first step. However, it is necessary to note that the selection affects correspondence between the computed and measured values.

To conduct the analyses efficiently, we created FE meshes for analyses of each frequency. The FE meshes were created to satisfy the requirement that $\lambda/d > 4.8$. Here, λ and d respectively denote wavelengths of upper limit frequencies of the octave band and the maximum nodal distance. The direct time integration method used here is a constant average acceleration method.

Table 2 lists DOFs, Δt, analysis time T and total time steps N_{step} as settings of the FE analysis. In addition, ρ and c were set respectively to 1.195 kg/m^3 and 342.3 m/s with consideration of the measured room's temperature.

All computations were performed on a server (eServer p5 model 595; IBM Corp.) with a 1.9 GHz processor (POWER5; IBM Corp.) located at Kyushu University. The respective amounts of memory required for the computations were 30 MB (125 Hz), 101 MB (250 Hz), and 748 MB (500 Hz).

On the other hand, when we calculate the impulse response using FDFEM with the inverse Fourier transform, the necessary memory for the FDFEM was 0.625 times that of the TDFEM. Theoretical estimations of memory required for the respective methods are presented in [9, 12, 21]. However, TDFEM presents the possibility of performing computations in less computational time than that of FDFEM, particularly for the high-frequency region and/or problems with many DOFs because the convergence property of the iterative solver applied on TDFEM is far better than that of FDFEM. The iterative solver converges within 20 iterations per time step, irrespective of the

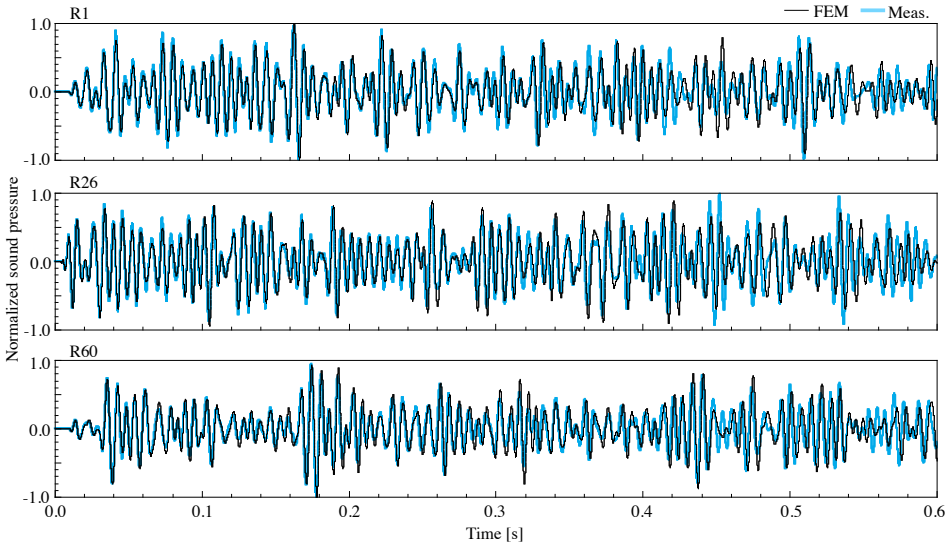

Figure 4: Comparisons of band-limited impulse responses (125 Hz) at receiving points R1, R26, and R60, as calculated using FEM and as obtained by measurement.

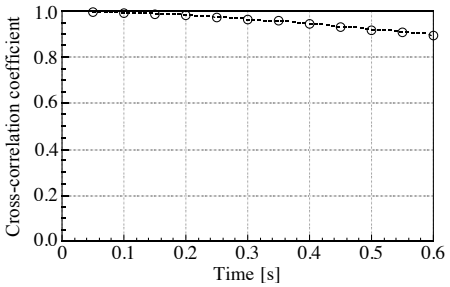

Figure 5: Spatial averaged cross-correlation coefficients of band-limited impulse responses, as calculated using FEM and as obtained by measurement.

sound field[12]. In addition, using IC(0) preconditioning, the iterative solver converges within five iterations[20]. On the other hand, the convergence property of the iterative solver applied on FDFEM depends strongly on the given sound field. Moreover, the method usually requires several thousand or more iterations per frequency for practical problems[21]. A comparison of the computational times required for TDFEM and FDFEM to obtain the same accurate result will be studied in the near future.

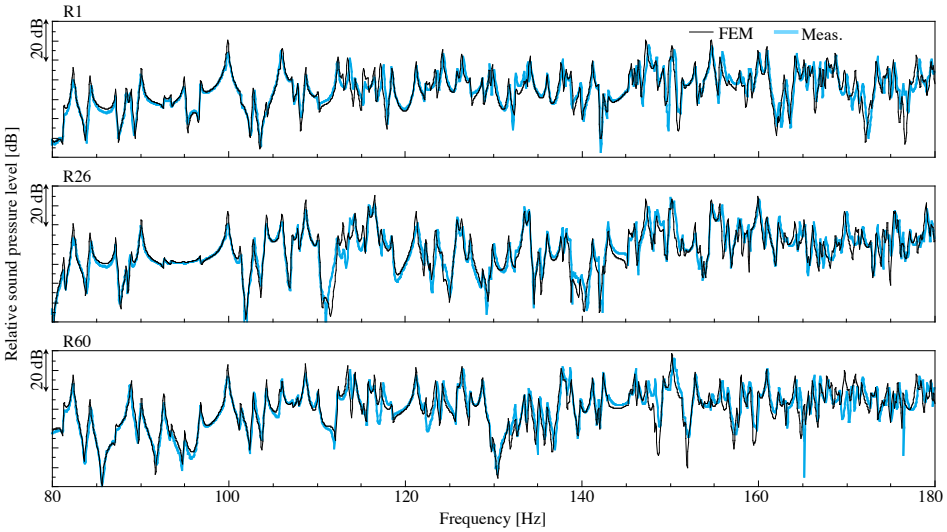

Figure 6: Comparisons of sound pressure levels at receiving points R1, R26, and R60, as calculated using FEM and as obtained by measurement.

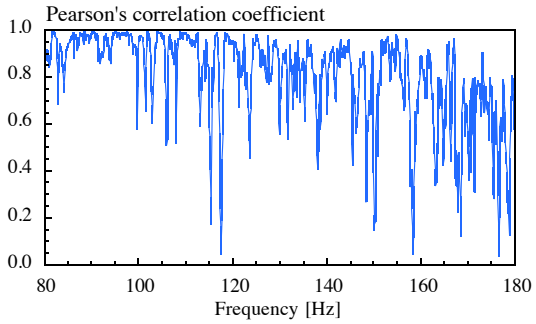

Figure 7: Pearson's correlation coefficients of sound pressure levels, as calculated using FEM and as obtained by measurement.

3.2. Results and discussion

Comparisons of the computed and the measured band-limited impulse responses with the octave band of 125 Hz at three receiving points R1, R26, and R60 at times up to 0.6 s are portrayed in Fig. 4. Here, frequency characteristics of the sound source in the measurement were measured in an anechoic room and convolved for the computed impulse responses. The measured impulse responses are filtered using an IIR filter (Butterworth type band pass filter) for comparison. The fine structures of the computed im-

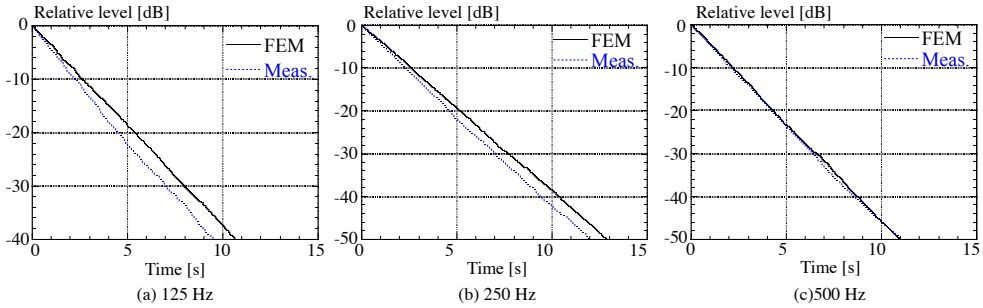

Figure 8: Comparisons of decay curves at receiving point R1, as calculated using FEM and as obtained by measurement: (a) 125 Hz, (b) 250 Hz, (c) 500 Hz.

pulse responses correspond closely to those of the measured ones, irrespective of receiving point. To evaluate the similarity between the measured and the computed impulse responses, the cross-correlation coefficient[22] between them is calculated with 0.05 s steps at all receiving points. Then its spatial averaged value is calculated using the cross-correlation coefficients. The spatial averaged cross-correlation coefficients are portrayed in Fig. 5. The value is 0.97 in the time up to 0.3 s and the value becomes 0.89 in the time up to 0.6 s. Although high correlation coefficients are obtained in the early time region, the value decreases over time, probably because of the influence of neglecting the loudspeaker cabinet in the computation and inaccuracy of the boundary condition. These factors might produce a phase difference between the responses, and an influence that accumulates over time.

Figure 6 presents comparisons of the computed and measured frequency responses obtained using the Fourier transform of the impulse responses. Overall, the computed results agree well with the measured results, irrespective of the receiving points. Figure 7 presents the Pearson's correlation coefficients between the computed and the measured sound pressure levels at all receiving points calculated for each frequency. The value averaged across frequency is 0.81.

For comparison of the decay properties of the computed and the measured band-limited impulse responses, the decay curve at a receiving point R1 calculated from the computed and the measured band-limited impulse response are shown in Fig. 8(a). Results show that attenuation of the measured sound pressures is greater than the computed values despite the fact that the agreement between both impulse responses is excellent in the early time region. The same result is obtained for other receiving points. To eval-

uate the agreement between the computed and the measured decay curves, the relative error norm $||e||_2$ is defined as

$$||e||_2 = \frac{||L_{\mathrm{FEM}}(t) - L_{\mathrm{Meas.}}(t)||_2}{||L_{\mathrm{Meas.}}(t)||_2} \times 100[\%], \tag{15}$$

where $L_{\mathrm{FEM}}(t)$ and $L_{\mathrm{Meas.}}(t)$, respectively, represent the relative level of decay curves at time t obtained by TDFEM and by measurements. The value of $||e||_2$ is calculated at all receiving points in the time region until $L_{\mathrm{FEM}}(t)$ at each receiving point decay to -35 dB, and its average value is calculated. The average value of $||e||_2$ is 13.4 % for 125 Hz. Furthermore, the spatially averaged reverberation times calculated from the computed and the measured band-limited impulse responses are, respectively, 16.68 s and 14.52 s. The relative error is 14.9%. Although a great difference is apparent for the decay curves and the reverberation times between the computation and the measurement, this is most likely the result of an improper setup of the impedances of the room surfaces in the computation. In other words, results indicate that the incident condition of acoustic wave to boundary surfaces is not completely random incidence for the 125 Hz frequency region. It is also indicated by the Schroeder frequency of the room. Therefore, we can expect improvement of correspondence between the computed and the measured decay curves and reverberation times in the higher frequency region as well.

Figures 8(b) and 8(c) depict a comparison of the computed and the measured decay curves at a receiving point R1 at 250 Hz and 500 Hz. As expected, results confirmed that correspondences between the computed and the measured decay curves for 250 Hz and 500 Hz are better than that of 125 Hz as the frequency becomes higher. The same result is obtained for other receiving points. The averaged values of $||e||_2$ are, respectively, 8.0% (250 Hz) and 3.3% (500 Hz). The spatial average values of the computed and the measured reverberation times are, respectively, 15.27 s and 14.25 s at 250 Hz; the relative error is 7.16 %. At 500 Hz, the spatial average values of the computed and the measured reverberation times are, respectively, 13.02 s and 12.77 s; the relative error is 1.96 %. From these results, the necessity of proper impedance setup of room surface corresponding to the actual incident condition of acoustic wave is shown for predicting the decay property of the actual room accurately.

Moreover, Fig. 9(a) depicts comparisons of the computed and measured band-limited impulse responses with octave bands of 250 Hz at receiving

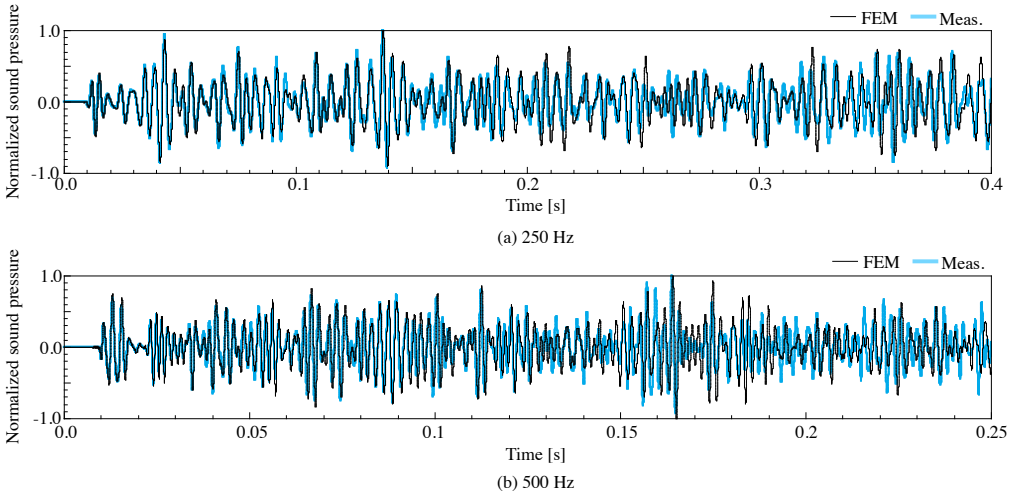

Figure 9: Comparison of band-limited impulse responses at receiving point R1, as calculated using FEM and as obtained by measurement: (a) 250 Hz and (b) 500 Hz.

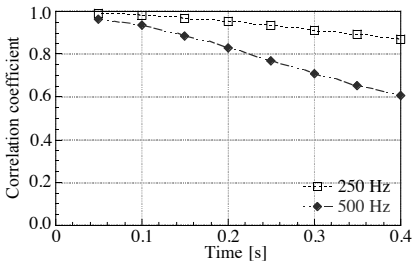

Figure 10: Spatial averaged cross-correlation coefficient of band-limited impulse responses, as calculated using FEM and as obtained by measurement: for 250 Hz and 500 Hz.

point R1 in the time region up to 0.4 s. Similarly, those of 500 Hz in the time up to 0.25 s are compared in Fig. 9(b). Overall, the agreement of the fine structure of the computed values and the measured values is excellent, irrespective of frequency. The same results are obtained for other receiving points. Figure 10 portrays the spatial averaged cross-correlation coefficients for each frequency. For 250 Hz, the value is 0.95 in the time up to 0.2 s and 0.87 in the time up to 0.4 s. Furthermore, for 500 Hz, the value becomes 0.93 in the time up to 0.1 s and 0.77 in the time up to 0.25 s. Again, the cross-correlation coefficients of each frequency decrease with time. In particular, the value decreases greatly for 500 Hz, probably for the same reason as that for 125 Hz. However, for 500 Hz, it seems that the main explanation for

the worse agreement in the early time region might be the lack of modeling the loudspeaker cabinet in the computations. In this frequency range, the wavelength of the 500 Hz is only about twice as large as the speaker diameter. Moreover, the loudspeaker is less and less omnidirectional as the frequency increases. This fact indicates that a point source modeling, with the inclusion of the loudspeaker's impulse response measured in one direction, does not work well for the higher frequencies. As a reference, averaged quantities of iterations per time step of absolute diagonal scaled COCG method are, respectively, 9.6 (125 Hz), 9.6 (250 Hz) and 10.6 (500 Hz). Good convergence characteristics were obtained for the analyses of all frequencies.

Based on these results, the basic accuracy and applicability of the TDFEM were demonstrated for diffused sound field with lightly damped surfaces. Additionally, appropriate boundary modeling is important to predict attributes of a sound field accurately, including the reverberation time of an actual room.

4. Conclusions

As described in this paper, an efficient TDFEM is presented. Then, the basic accuracy and the applicability of the TDFEM for sound field analysis in architectural spaces are demonstrated through comparisons between computed and the measured results of sound fields in an irregularly shaped reverberation room with volume of 166 m^3 at frequencies of 125–500 Hz. For all frequencies, the fine structure of the computed band-limited impulse responses agree well with measured ones in the early time region up to 0.1 s, with the value of the cross correlation coefficient greater than 0.93. Moreover, the values of the cross correlation coefficient decrease gradually over time; and more rapidly for higher frequencies. Furthermore, the computed decay curves and reverberation times agree well with the measured ones, and with a better fit the higher the frequency (up to 500 Hz). Investigations of the accuracy and applicability of the TDFEM for more practical rooms with complicated boundary conditions are now underway.

Acknowledgement

We thank Tatsuya Imai, master's course student, for important cooperative contributions to this research. This work was partly supported by a

Grant-in-Aid for Science Research (A) 19206062 from the Japan Society for Promotion of Science.

References

[1] D. Botteldooren, Finite-difference time-domain simulation of low-frequency room acoustic problems. J. Acoust. Soc. Am. 98(6) (1995) 3302-3308.

[2] J. LoVetri, D. Mardare, G. Soulodre, Modeling of the seat dip effect using the finite-difference time-domain method, J. Acoust. Soc. Am. 100(4) (1996) 2204-2212.

[3] S. Sakamoto, H. Nagatomo, A. Ushiyama, H. Tachibana, Calculation of impulse responses and acoustic parameters in a hall by the finite-difference time-domain method, Acoust. Sci. Tech. 29(4) (2008) 256-265.

[4] S. Choi, H. Tachibana, Estimation of impulse response in a room by the finite element method, J. Acoust. Soc. Jpn. 49(5) (1993) 328-333.

[5] V. Easwaran, A. Craggs, Transient response of lightly damped rooms: A finite element approach, J. Acoust. Soc. Am. 99(1) (1996) 108-113.

[6] V. Easwaran, A. Craggs, An application of acoustic finite element models to finding the reverberation times of irregular rooms, Acust. acta Acust. 82 (1996) 54-64.

[7] T. Otsuru, K. Fujii, Finite elemental analysis of sound field in rooms with sound absorbing materials, Proc. Inter-noise 94 (1994) 2011-2014.

[8] M. Serikawa, H. Takeuchi, T. Katayama, A. Taguchi, Transient analysis of three dimensional acoustic field by finite element method, J. Acoust. Soc. Jpn. 52(9) (1996) 680-687.

[9] T. Okuzono, T. Sueyoshi, T. Otsuru, N. Okamoto, R. Tomiku, Time domain finite element sound field analysis of rooms using iterative methods and parallelization. Proc. Inter-noise 2006 on CD-ROM, 2006.

[10] T. Otsuru, R. Tomiku, Basic characteristics and accuracy of acoustic element using spline function in finite element sound field analysis, Acoust. Sci. Tech. 21(2) (2000) 87-95.

[11] S. Marburg, B. Nolte, Computational Acoustic of Noise Propagation in Fluids – Finite and Boundary Element Methods, Springer, 2008.

[12] T. Okuzono, T. Otsuru, N. Okamoto, R. Tomiku, Sound field analysis of rooms by time domain finite element method with an iterative method, J. Environ. Eng. (Trans. of AIJ) No. 628 (2008) 701-706.

[13] N.M. Newmark, A method of computation for structural dynamics, J. Eng. Mech. Div. 85 (1959) 67-94.

[14] T.J.R. Hughes, The Finite Element Method Linear Static and Dynamic Finite Element Analysis, Dover, 2000.

[15] H.A. van der Vorst, J. Melissen, A Petrov–Galerkin type method for solving $Ax = b$, where A is symmetric complex, IEEE Trans. on Magn. 26(2) (1990) 706-708.

[16] Moethuthu, N. Okamoto, A. Shiode, M. Kakihara, S. Fujino, T. Otsuru, A particular preconditioning technique for symmetric complex matrix, Information 10(2) (2007) 193-198.

[17] Y. Suzuki, F. Asano, H. Kim, T. Sone, An optimum computer-generated pulse signal suitable for the measurement of very long impulse responses, J. Acoust. Soc. Am. 97(2) (1995) 1119-1123.

[18] F. Satoh, J. Hirano, S. Sakamoto, H. Tachibana, Sound propagation measurement using swept-sine signal, Proc. Inter-noise 2005 on CD-ROM, No.1691 (2005).

[19] A. London, The determination of reverberant sound absorption coefficients from acoustic impedance measurements, J. Acoust. Soc. Am. 22(2) (1950) 263-269.

[20] T. Okuzono, T. Otsuru, R. Tomiku, N. Okamoto, Speedup of time domain finite element sound field analysis of rooms, Proc. Inter-noise 2008 on CD-ROM, No.0877 (2008).

[21] N. Okamoto, R. Tomiku, T. Otsuru, Y. Yasuda, Numerical analysis of large-scale sound fields using iterative methods part Ⅱ: Application of Krylov subspace methods to finite element analysis, J. Comp. Acoust. 15(4) (2007) 473-493.

[22] Z. Maekawa, P. Load, Environmental and architectural acoustics, E. & FN SPON. Chap 10.3 (1993) 317.